Indian Journal of Pure & Applied Physics
Vol. 55, January 2017, pp. 43-59

Vibrational (FT-IR and FT-Raman) spectra and quantum chemical studies on the molecular structure of p-hydroxy-N-(p-methoxy benzylidene) aniline

B Revathi[a], V Balachandran[a]*, B Raja[b] & K Anitha[c]

[a]Centre for Research, Department of Physics, Arignar Anna Government Arts College, Musiri, Tiruchirappalli 621 211, India
[b]Department of Physics, Government Arts College, Kulithalai, Karur 639 120, India
[c]Department of Physics, Bharathidasan University Constitutent College, Lalgudi, Tiruchirappalli 621 601, India

Received 10 June 2016; revised 28 September 2016; accepted 17 November 2016

The FT-IR and FT-Raman spectra of p-hydroxy-N-(p-methoxy benzylidene) aniline have been recorded in the region 4000-400 cm^{-1} and 3500-100 cm^{-1}, respectively. The optimized molecular geometry, vibrational frequencies in ground state have been calculated using density functional B3LYP methods (DFT) with 6-31+G(d,p) and 6-311++G(d,p) basis sets. The observed FT-IR and FT-Raman vibrational frequencies have been analysed and compared with theoretically predicted vibrational frequencies. The geometries and normal modes of vibration obtained from B3LYP/6-311+G(d,p) and B3LYP/6-311++G(d,p) methods are reliable compared with the experimental data. The natural bonding orbital (NBO) analysis of the investigated molecule have been computed using DFT/ B3LYP/6-311++G(d,p) calculations. The calculated HOMO and LUMO energies show that charge transfer occurs within molecule.

Keywords: Vibrational spectra, p-Hydroxy-N-(p-methoxy benzylidene) aniline, First order hyperpolarizability, HOMO–LUMO, Charge transfer

1 Introduction

Aromatic amines are very important in chemical industries. Aniline and its derivatives have been widely used as starting materials in a vast amount of chemicals, pharmaceuticals, dyes, electro-optical and many other industrial processes[1-5]. The conducting polymers of aniline are used as diodes and transistors[6-9]. Particularly, aniline and its derivatives are used in the production of dyes, pesticides and antioxidants. 4-chloro-2-methylaniline and 4-chloro-3-methylaniline and its hydrochlorides were commercially used as intermediates in the manufacture of azo dyes, aromatic amino sulphonic acids and chlordane form an insecticide[10,11]. Some of the *p*-substituted derivatives of aniline are local anesthetics, and in these molecules the amino group plays an important role in the interaction with the corresponding receptor. The understanding of their structure, molecular properties as well as nature of reaction mechanism, they undergo, has great importance and has been the subject of many experimental and theoretical studies. A systematic study on the vibrational spectra of simple primary, secondary and tertiary anilines received considerable attention in the spectroscopic literature in view of their industrial significance. The introduction of one or more substituents in aniline leads to the variation of charge distribution in the molecules, and consequently, this greatly affects the structural, electronic and vibrational parameters[12]. The methyl and amino groups are generally referred as electron donating substituents in aromatic ring systems.

The methyl group interacts with the aromatic ring system through hyper conjugation, while the amino group shares its lone pair electrons with the ring and induces delocalization of π-electrons. Both the effects imply electronic delocalization and are taken into account by the molecular orbital approach[13,14]. The position of the substituent in the benzene ring as well as its electron donor/acceptor capabilities plays a very important role on the structural and electronic properties of the molecules.

The molecular geometrical structure changes due to enhanced interaction between the aromatic ring, the methyl and amino groups[15]. The methyl group in compound makes it around 25 times more reactive than benzene in such pharmalogical action.

Vibrational assignment based FT-IR in the vapour solution liquid phases and the Raman spectra in the liquid state have been reported for aniline[16]. The molecular structure of aniline is also known in the gas phase from microwave spectroscopy[17,18] and in the solid state from X-ray crystallography[19].

* Corresponding author (E–mail: brsbala@rediffmail.com)

Vibrational analysis has been reported theoretically using semi-empirical[20,21] *ab initio* methods[20-23]. Extensive recent studies on vibrational spectra of substituted anilines assigned[24,25-29] complete vibrational mode and frequency analysis. Vibrational modes and frequencies analysis of m-methyl aniline have been studied by Altun *et al.*[24]. Assignments of some bands observed in the infrared spectrum of p-methyl aniline are given in literature[30-34]. The vibrational spectra of fluoro methylaniline[35] and chloro methylaniline[36] have been reported. Shankar *et al.*[37] studied 2-chlro-6-methylaniline with polarized Raman and infrared spectra. Barluenga *et al.*[38] synthesized and studied 1H and13C NMR spectra of 2-chloro-N-methylaniline. Recently Rai *et al.*[39] performed IR, Raman spectral studied and DFT calculations of chlorine substituted anilines. Overtone spectra of 2-ethylaniline, N-methylaniline, N-ethylaniline, N-N-dimethyl aniline and N-N-di ethyl aniline have been studied in region 2500-1500 cm^{-1} by Rai *et al.*[40]. Potentially useful NLO material N-(p-methoxy benzylidene) aniline has been studied by DFT computations and spectroscopic analysis by Balachandran *et al.*[1].

In the present study, we have proposed the vibrational assignments of p-hydroxy-N-(p-methoxy benzylidene) aniline (pHNpMBA) according to the characteristics frequencies observed in FT-IR and FT-Raman spectra. Furthermore, we interpreted the calculated spectra in terms of potential energy distribution (PEDs) and also made the vibrational assignments based on these PED results. In addition to that the molecular species which are responsible for chemical stability and chemical reactivity of the molecule were also identified by NBO and MEP surface analysis, respectively. The electric dipole moment (μ) and first hyper polarizability (β) values of the investigated molecule were computed using density functional theory calculations. The calculated results also show that the pHNpMBA molecule might have microscopic non-linear optical (NLO) behaviour with non-zero values. Furthermore, the intensities of molecular vibrations at different temperatures were examined on basis of correlation graphs. To the best of our knowledge, these have been no other significant studies reported for considering of pHNpMBA so far. This inadequacy observed in the literature encouraged us to make the aforementioned studies in this work.

2 Experimental Study

The molecule pHNpMBA was provided by the Lancaster Chemical Company, (UK), and it was used as such without further purification. The room temperature FT-IR spectrum of pHNpMBA was recorded in the frequency region 4000–400 cm^{-1} at a resolution of ±1 cm^{-1} using BRUKER IFS 66V FTIR spectrometer equipped with an MCT detector, a KBr beam splitter and globar source. The FT-Raman spectrum of MBA was recorded on a computer interfaced BRUKER IFS 66V model interferometer equipped with FRA-106 FT-Raman accessories. The spectrum was measured in the Stokes region 3500-100 cm^{-1} using Nd:YAG laser at 1064 nm of 200 mW output as the excitation source and with a liquid nitrogen-cooled Ge-diode detector with the powder sample in a capillary tube. 100 scans were accumulated to increase the signal-to-noise ratio with a total registration time of about 30 min. The reported wave numbers are expected to be accurate within ±1 cm^{-1}. A correction according to the fourth-power scattering factor was performed, but no instrumental correction was made.

3 Computational Details

The density functional theory computations were performed with the aid of GAUSSIAN 09W software package[41] with internally stored B3LYP/6-31+G(d,p) and B3LYP/6-311++G(d,p) basis sets. At first, the global minimum energy structure of the title molecule was optimized by both the aforesaid basis set methods. Subsequently, the vibrational normal mode wave numbers in association with the molecule were derived along with their IR intensity and Raman activity.

In our calculations, there were some deviations persist between the observed and calculated wave numbers due to the neglect of anharmonic effect at the beginning of frequency calculation and basis set deficiencies. In the present study, these deviations were overcome by a selective scaling procedure in the natural internal coordinate representation followed by other studies[42,43]. Transformations of the force field and the subsequent normal coordinate analysis including the least squares refinement of the scaling factors, calculation of potential energy distribution (PED) and IR and Raman intensities were done on a PC with the MOLVIB program (Version V7.0-G77) written by Sundius[44–46]. The PED elements provide a measure of each internal coordinate's contribution to the normal coordinate. For the plots of simulated IR and Raman spectra, pure Lorentzian band shapes were used with a bandwidth of 10 cm^{-1} and the modified Raman activities during scaling procedure with MOLVIB were converted to relative Raman intensities using the following relationship derived from the basic theory of Raman scattering[47–49]. Finally, the converted

Raman intensities and the calculated infrared intensities were modified by assigning the highest intensity peak to 100%:

$$I_i = \frac{f(v_0 - v_i)^4 s_i}{v_i\left[1 - \exp\left(\frac{-hcv_i}{k_b T}\right)\right]}$$

where v_0 is the exciting wave number (1064 nm = 9398 cm^{-1}) of laser light source used while recording Raman spectra, v_i the vibrational wave number of the i^{th} normal mode. *h, c* and K_b fundamental constants, and *f* is a suitably chosen common normalization factor for all peak intensities of the Raman spectrum of the title molecule. In order to predict the reactive behaviour of the molecule, we have plotted MEP surface and derived electrostatic potential values and point charges at B3LYP/6-311++G(d,p) basis set. From the computed NBO results, the stabilization energies of molecular species which are most responsible for the stability of molecule were identified. Furthermore, the highest occupied molecular orbital (HOMO) and the lowest unoccupied molecular orbital (LUMO) energies were predicted to interpret the orbital overlapping and the possibility of charge transfer within the molecule using B3LYP method with B3LYP/6-311++G(d,p) basis set combination.

4 Results and Discussion

4.1 Molecular geometry

In order to find most optimized geometry, the energy calculations are carried out for various possible conformers. The eight possible conformers of the title compound are shown in Fig. 1. The global minimum energy were carried out using B3LYP/6-31+G(d,p) and B3LYP/6-311++G(d,p) basis sets for eight conformers. The calculated energies for all conformers are presented in Table 1. From DFT calculations using B3LYP/6-311++G(d,p) basis set the conformer C4 (Fig. 2) is predicted to be -746.5029

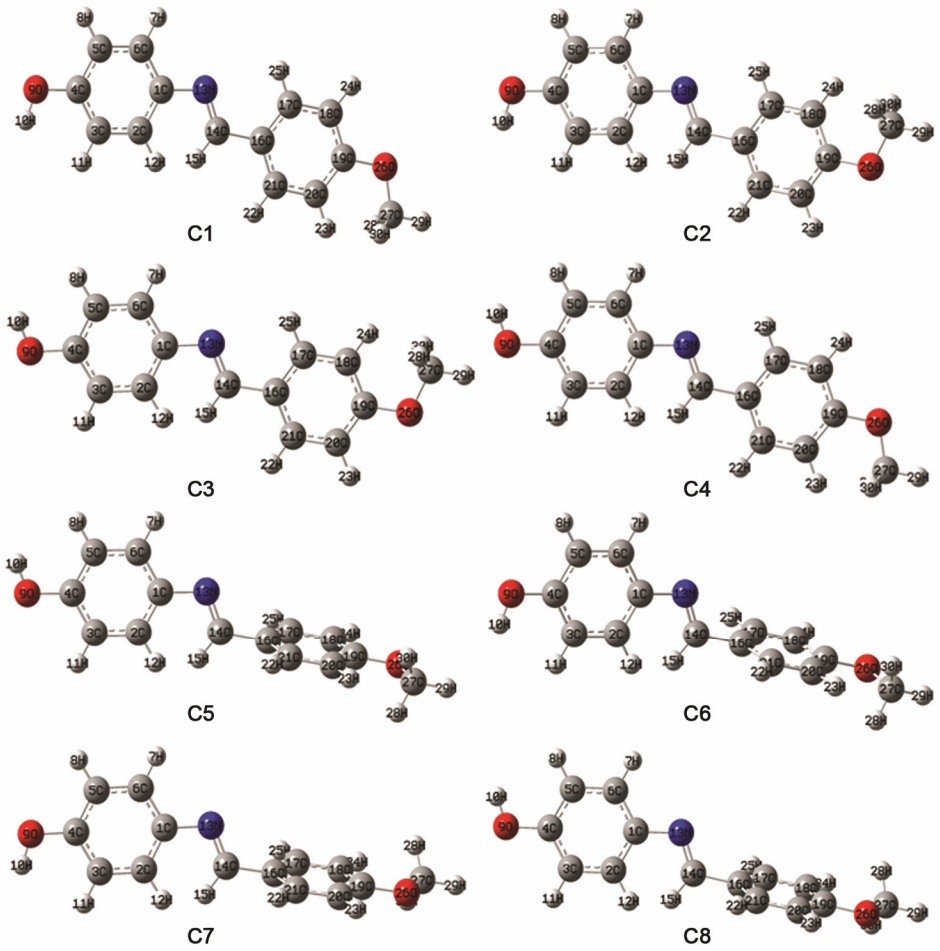

Fig. 1 – Various possible conformers of p-hydroxy-N-(p-methoxybenzylidene)aniline

Table 1 – Calculated energy for p-hydroxy-N-(p-methoxybenzylidene) aniline by B3LYP/6-31+G(d,p) and B3LYP /6-311++G(d,p)

Conformer	Energy			
	B3LYP/6-31+G(d,p)		B3LYP/6-311++G(d,p)	
	Hartrees	kJ/mole	Hartrees	kJ/mole
C1	-746.5024	-1959942.2987	-746.6555	-1960344.2427
C2	-746.5025	-1959942.3621	-746.6556	-1960344.2719
C3	-746.5027	-1959942.8768	-746.6557	-1960344.7778
C4	-746.5029	-1959942.9675	-746.6558	-1960344.8957
C5	-746.4920	-1959914.8675	-746.6452	-1960317.0719
C6	-746.4918	-1959914.3375	-746.6449	-1960316.4155
C7	-746.4918	-1959914.4728	-746.6450	-1960316.5746
C8	-746.4920	-1959914.9668	-746.6452	-1960317.1967

C4: Global minimum energy

Hartrees (-1959942.9675 kJ/mole) more stable than the other conformers. As clearly seen from the values given in Table 1, the basis set size effect on the calculated energies is not so much, but of considerable importance; use of the basis sets of larger sizes gives rise to slight increases in the differences; however, unstable conformers give rise to decreases in the differences between the calculated energies.

The geometry of the molecules under investigation is considered by possessing C_1 point group symmetry. The 84 fundamental modes of vibrations of compound are distributed into the irreducible representations under C_1 symmetry as 57 in-plane vibrations of and 27 out of plane vibrations of A' species.

Normal co-ordinate analysis is the mathematical procedure that gives the normal co-ordinates their frequencies and force constants. The detailed description of vibrational modes can be given by means of normal co-ordinate analysis. The internal co-ordinates describe the position of the atoms in terms of distances, angles and dihedral angles with respect to an origin atom. The symmetry co-ordinates are constructed using the set of internal co-ordinates. In this study, the full set of 108 standard internal co-ordinates (containing 27 redundancies) for pHNpMBA was defined as given in Table 2. From those a non-redundant set of local symmetry co-ordinates were constructed by suitable linear combinations of internal co-ordinates are presented in Table 3.

The optimized molecular structure (conformer C4) of the pHNpMBA compound is shown in Fig. 2 with numbering of the atoms. The optimized bond lengths and bond angles of pHNpMBA calculated by B3LYP method using 6-31+G(d,p) and 6-311++G(d,p) basis set are listed in Table 2, in accordance with atom numbering scheme as shown in Fig. 1. Our optimized structural parameters are now compared with the exact experimental X-ray data for 4-chloro 2-methyl

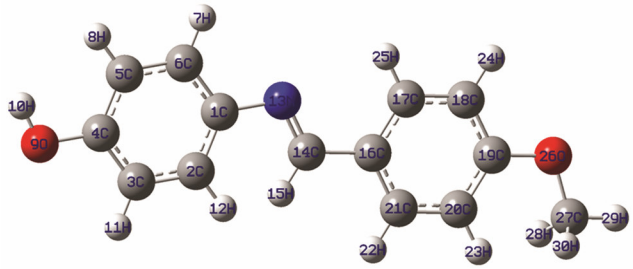

Fig. 2 – Optimized molecular structure of p-hydroxy-N-(p-methoxybenzylidene)aniline

aniline and 4-benzylidene amino antipyrine[50,51] and the theoretical values of N-(p-methoxy benzylidene) aniline[1] are shown in Table 4, it is shown that the various bond lengths are found to be more or less than experiment. This overestimation can be explained that the theoretical calculations belong to isolated molecule in gaseous phase and the experimental results belong to similar molecules in solid state.

Several researches[52,53] have explained the changes in the frequency or bond length of the C–H bond on substitution due to a change in the charge distribution on the carbon atom of the benzene ring. The carbon atoms are bonded to the hydrogen atoms with σ bond in benzene and substitution of an aniline group for hydrogen reduces the electron density at the ring carbon atom. The ring carbon atoms in substituted benzenes exert a large attraction on the valance electron cloud of the hydrogen atom resulting in an increase in the C–H force constant and a decrease in the corresponding bond length. The reverse holds well on substitution with electron denoting groups. The actual change in the C–H bond length would be influenced by the combined effects of the inductive mesomeric interaction and the electric dipole field of the polar subsistent. In this study, the C–H bond lengths were calculated as 1.0856, 1.0814, 1.0834 and 1.0833 by B3LYP/6-311++G(d,p) for the ring.

The optimized parameters obtained by B3LYP method using different basis sets are approximately smaller than those observed experimentally. At, all levels reported here, the calculated bond length and angle at the very close to the experimental values, except for the ring angle at the point of substitution. With an electron donating and electron-with drawing substituents at the para positions the symmetry of the benzene ring is distorted, yielding ring angles smaller than 120˚ at the point substitution and slightly longer than 120° at the ortho and meta position. Similar values found to be present in other aniline derivatives which are m-methylaniline[24], o-methyaniline[54] and

Table 2 – Internal coordinates p-hydroxy-N-(p-methoxybenzylidene)aniline

No. (i)	Symbol	Type	Definition
1-9	t_i	C-H	C_5-H_8, C_6-H_7, C_2-H_{12}, C_3-H_{11}, C_{14}-H_{15}, C_{17}-H_{25},C_{18}-H_{24},C_{21}-H_{22}, C_{20}-H_{23}
10-12	t_i	C-H	C_{27}-H_{28}, C_{27}-H_{27},C_{27}-H_{30}
13-25	R_i	C-C	C_1-C_2, C_2-C_3, C_3-C_4, C_4-C_5, C_5-C_6, C_6-C_1, C_{14}-C_{16}, C_{16}-C_{17}, C_{17}-C_{18}, C_{18}-$C_{19,}$ C_{19}-C_{20}, C_{20}-C_{21}, C_{21}-C_{16}
26-27	P_i	C-N	C_1-N_{13}, C_{14}-N_{13}
28-30	r_i	C-O	C_4-O_9, C_{19}-O_{26}, C_{27}-O_{26}
31	T_i	O-H	O_9-H_{10}
32-37	α_{ii}	Ring1	C_1-C_2-C_3, C_2-C_3-C_4, C_3-C_4-C_5, C_4-C_5-C_6, C_5-C_6-C_1, C_6-C_1-C_2
38-43	αi_i	Ring2	C_{16}-C_{17}-C_{18}, C_{17}-C_{18}-C_{19}, C_{18}-C_{19}-C_{20}, C_{19}-C_{20}-C_{21}, C_{20}-C_{21}-C_{16}, C_{21}-C_{16}-C_{17}
44	β_i	C-O-H	C_4-O_9-H_{10}
45-52	γ_i	C-C-H	C_4-C_5-H_8, C_6-C_5-H_8, C_5-C_6-H_7, C_1-C_6-H_7, C_1-C_2-H_{12},C_3-C_2-H_{12}, C_2-C_3-H_{11},C_4-C_3-H_{11}
53-60	γ_i	C-C-H	C_{16}-C_{17}-H_{25}, C_{18}-C_{17}-C_{25}, C_{17}-C_{18}-H_{24}, C_{19}-C_{18}-H_{24}, C_{19}-C_{20}-H_{23}, C_{21}-C_{20}-H_{23}, C_{20}-C_{21}-H_{22}, C_{16}-C_{21}-H_{22}
61-62	δ_i	C-C-N	C_2-C_1-N_{13}, C_6-C_1-N_{13}
63	Π_i	C-C-N	C_{16}-C_{14}-N_{13}
64	ρ_i	N-C-H	N_{13}-C_{14}-H_{15}
65	γ_i	C-C-H	C_{16}-C_{14}-H_{15}
66-69	σ_i	C-C-O	C_{18}-C_{19}-C_{26}, C_{20}-C_{19}-O_{26}, C_3-C_4-O_9, C_5-C_4-O_9
70	ψ_i	C-O-C	C_{19}-O_{26}-C_{27}
71-73	ϕ_i	O-C-H	O_{26}-C_{27}-H_{28}, C_{26}-C_{27}-H_{29}, C_{26}-C_{27}-H_{30}
74-76	Δ_i	H-C-H	H_{28}-C_{27}-H_{29}, H_{28}-C_{27}-H_{30}, H_{29}-C_{27}-H_{30}
77-82	ω_i	Ring1	C_1-C_2-C_3-C_4, C_2-C_3-C_4-C_5, C_3-C_4-C_5-C_6, C_4-C_5-C_6-C_1,C_5-C_6-C_1-C_2, C_6-C_1-C_2-C_3
83-88	ω_i	Ring2	C_{16}-C_{17}-C_{18}-C_{19}, C_{17}-C_{18}-C_{19}-C_{20}, C_{18}-C_{19}-C_{20}-C_{21}, C_{19}-C_{20}-C_{21}-C_{16}, C_{20}-C_{21}-C_{16}-C_{17}, C_{21}-C_{16}-C_{17}-C_{18}
89-92	ω_i	C-H	H_7-C_6-C_5-C_1, H_{12}-C_2-C_1-C_3, H_{11}-C_3-C_2-C_4, H_8-C_5-C_6-C_4
93-96	ω_i	C-H	H_{25}-C_{17}-C_{16}-C_{18}, H_{24}-C_{18}-C_{17}-C_{19}, H_{23}-C_{20}-C_{19}-C_{21}, H_{22}-C_{21}-C_{20}-C_{16}
97-98	ω_i	O-C	O_9-C_4-C_5-C_3 , O_{26}-C_{19}-C_{18}-C_{20}
99	ω_i	C-N	N_{13}-C_1-C_2-C_6
100	ω_i		C_{14}-N_{13}-C_1-C_2(C_6)
101	ω_i	C-H	H_{15}-C_{14}-N_{13}-C_{16}
102-104	τ_i	C-O	C_{19}-O_{26}-C_{27}-H_{28},C_{19}-O_{26}-C_{27}-H_{29},C_{19}-O_{26}-C_{27}-H_{30}
105	ω_i	C-N	C_1-N_{13}-C_{14}-H_{15},
106	ω_i	C-C	C_{17}-C_{16}.C_{14}-H_{15}
107	ω_i	C-N	C_1-N_{13}-C_{14}-C_{16}
108	ω_i	O-H	H_{10}-O_9-C_6-C_3(C_5)

p-methyl aniline. The C_1–N_{13} and C_{14}–N_{13} bond distance of ca 1.41 and 1.27 is just 0.01 Å lower than the reported experimental values of 1.42 Å.

4.2 First hyperpolarizability

NLO effects arise from the interactions of electromagnetic fields in various media to produce new fields altered in phase, frequency, amplitude or other propagation characteristics' from the incident fields[55]. NLO is at the forefront of current research because of its importance in providing the key functions of frequency shifting, optical modulation, optical switching, optical logic, and optical memory for the emerging technologies in areas such as telecommunications, signal processing, and optical interconnections[56–59].

The first hyperpolarizability (β) of this novel molecular system, and the related properties (β, α_0 and Δα) were calculated based on the finite-field approach. In the presence of an applied electric field, the energy of a system is a function of the electric field. Polarizability and hyperpolarizability characterize the response of a system in an applied electric field[60]. They determine not only the strength of molecular interactions (long-range interaction, dispersion force, etc.) and the cross sections of different scattering and collision process but also the NLO properties of the system[61,62]. First hyperpolarizability is a third rank tensor that can be described by a 3×3×3 matrix. The 27 components of the 3D matrix can be reduced to 10 components due to the Kleinman symmetry[63] and can be given in the lower tetrahedral format. It is obvious that the lower part of the 3×3×3 matrices is tetrahedral. The components are defined as the coefficients in the Taylor series, with expansion of the energy in the external electric field. When the external electric field is weak and homogeneous, this expansion becomes:

$$E = E^0 - \mu_\alpha F_\alpha - \frac{1}{2}\alpha_{\alpha\beta} F_\alpha F_\beta - \frac{1}{6}\beta_{\alpha\beta\gamma} F_\alpha F_\beta F_\gamma + \ldots$$

Table 3 – Local symmetry coordinates of p-hydroxy-N-(p-methoxybenzylidene)aniline

No. (i)	Symbol	Definition
-9	CH	$t_1,t_2,t_3,t_4,t_5,t_6,t_7,t_8,t_9$
10	CH_{3ss}	$(t_{10}+t_{11}+t_{12})/\sqrt{3}$
11	CH_{3ips}	$(2t_{10}-t_{11}-t_{12})/\sqrt{6}$
12	CH_{3ops}	$(t_{11}-t_{12})/\sqrt{2}$
13-25	CC	R_{13}, R_{14}, R_{15}, R_{16}, R_{17}, R_{18}, R_{19}, R_{20}, R_{21}, R_{22}, R_{23}, R_{24}, R_{25}
26-27	CN	P_{26},P_{27}
28-30	CO	r_{28},r_{29},r_{30}
31	OH	T_{31}
32	$R1_{trigd}$	$(\alpha_{32}-\alpha_{33}+\alpha_{34}-\alpha_{35}+\alpha_{36}-\alpha_{37})/\sqrt{6}$
33	$R1_{symd}$	$(-\alpha_{32}-\alpha_{33}+2\alpha_{34}-\alpha_{35}-\alpha_{36}+2\alpha_{37})/\sqrt{2}$
34	$R1_{asymd}$	$(\alpha_{32}-\alpha_{33}+\alpha_{35}-\alpha_{36})/\sqrt{2}$
35	$R2_{trigd}$	$(\alpha_{38}-\alpha_{39}+\alpha_{40}-\alpha_{41}+\alpha_{42}-\alpha_{43})/\sqrt{6}$
36	$R2_{symd}$	$(-\alpha_{38}-\alpha_{39}+2\alpha_{40}-\alpha_{41}-\alpha_{42}+2\alpha_{43})/\sqrt{12}$
37	$R2_{asymd}$	$(\alpha_{38}-\alpha_{39}+\alpha_{41}-\alpha_{42})/\sqrt{2}$
38	CO	β_{44}
39-46	CH	$(\gamma_{45}-\gamma_{46})/\sqrt{2}$, $(\gamma_{47}-\gamma_{48})/2$,$(\gamma_{49}-\gamma_{50})/\sqrt{2}$, $(\gamma_{51}-\gamma_{52})/\sqrt{2}$, $(\gamma_{53}-\gamma_{54})/\sqrt{2}$, $(\gamma_{55}-\gamma_{56})/\sqrt{2}$,$(\gamma_{57}-\gamma_{58})/2$,$(\gamma_{59}-\gamma_{60})/\sqrt{2}$
47	CN	$(\delta_{61}-\delta_{62})/\sqrt{2}$
48	CN	π_{63}
49	CN	ρ_{64}
50	CH	γ_{65}
51-52	CC	$(\sigma_{66}-\sigma_{67})/\sqrt{2}$, $(\sigma_{68}-\sigma_{69})/\sqrt{2}$
53	CO	ψ_{70}
54	$CH3_{sb}$	$(-\phi_{71}-\phi_{72}-\phi_{73}+\Delta_{74}+\Delta_{75}+\Delta_{76})/\sqrt{6}$
55	$Ch3_{ipb}$	$(-\Delta_{74}+\Delta_{75}+2\Delta_{70})/\sqrt{6}$
56	$Ch3_{opb}$	$(-\Delta_{74}-\Delta_{76})/\sqrt{2}$
57	$CH3_{ipr}$	$(2\phi_{71}-\phi_{72}-\phi_{73})/\sqrt{6}$
58	$Ch3_{opr}$	$(\phi_{72}-\phi_{73})/\sqrt{2}$
59	$tR1_{trig}$	$(\omega_{77}+\omega_{78}+\omega_{79}+\omega_{80}+\omega_{81}+\omega_{82})/\sqrt{6}$
60	$tR1_{sym}$	$(\omega_{77}+\omega_{79}+\omega_{80}+\omega_{82})$
61	$tR1_{asym}$	$(-\omega_{77}+2\omega_{78}-\omega_{79}+\omega_{80}+2\omega_{81}-\omega_{82})\sqrt{12}$
62	$tR2_{trig}$	$(\omega_{83}+\omega_{84}+\omega_{85}+\omega_{86}+\omega_{87}+\omega_{88})/\sqrt{6}$
63	$tR2_{sym}$	$(-\omega_{83}+\omega_{85}+\omega_{86}+\omega_{88})$
64	$tR2_{asym}$	$(-\omega_{83}+2\omega_{84}-\omega_{85}+\omega_{80}+2\omega_{87}-\omega_{88})\sqrt{12}$
65-72	ωCH	ω_{89}, ω_{90}, ω_{91}, ω_{92}, ω_{93}, ω_{94}, ω_{95}, ω_{96}
73-74	ωOC	ω_{97}, ω_{98}
75-76	ωCN	ω_{99}, ω_{100}
77	ωCH	ω_{101}
78-80	τCO	τ_{102}, τ_{103}, τ_{104}
81	ωCN	ω_{105}
82	ωCC	ω_{106}
83	ωCN	ω_{107}
84	ωOH	ω_{108}

where E^0 is the energy of the unperturbed molecules F_α is the field at the origin, μ_α, $\alpha_{\alpha\beta}$ and $\beta_{\alpha\beta\gamma}$ are the components of the dipole moment, polarizability and the first hyperpolarizabilities, respectively. The total static dipole moment μ, the mean polarizability α, the anisotropy of the polarizability $\Delta\alpha$, and the mean first hyperpolarizability β, are defined as follows using the *x, y, z* components:

$$\mu = \left(\mu_x^2 + \mu_y^2 + \mu_z^2\right)^{1/2}$$

$$\langle\alpha\rangle = \frac{\alpha_{xx} + \alpha_{yy} + \alpha_{zz}}{3}$$

$$\Delta\alpha = \left\{ \frac{\left(\alpha_{xx}-\alpha_{yy}\right)^2 + \left(\alpha_{xx}-\alpha_{zz}\right)^2 + \left(\alpha_{zz}-\alpha_{yy}\right)^2 + 6\left(\alpha_{xz}^2 + \alpha_{yz}^2 + \alpha_{xy}^2\right)}{2} \right\}^{1/2}$$

Table 4 – Optimized molecular geometrical parameters of p-hydroxy-N-(p-methoxy benzylidene)aniline

Parameters	Bond lengths (Å)				Parameters	Bond angles (°)			
	Experimental*	Ref.#	*A*	*B*		Experimental*	Ref.#	*A*	*B*
C1-C2	1.39	1.40	1.39	1.41	C2-C1-C6	117.5	120.16	118.74	118.14
C1-C6		1.40	1.39	1.40	C2-C1-N13		120.32	117.34	123.97
C1-N13	1.42	1.41	1.41	1.41	C6-C1-N13		118.33	123.90	117.83
C2-C3	1.39	1.39	1.38	1.39	C1-C2-C3	123.2	119.28	120.95	121.05
C2-H12	1.08	1.08	1.07	1.08	C1-C2-H12	120.3	119.17	118.35	119.78
C3-C4	1.43	1.39	1.39	1.40	C3-C2-H12		120.71	120.70	119.14
C3-H11	1.08	1.08	1.07	1.08	C2-C3-C4		119.39	119.63	119.98
C4-C5		1.39	1.38	1.40	C2-C3-H11		120.05	121.52	121.02
C4-O9			1.38	1.37	C4-C3-H11		119.31	118.84	118.99
C5-C6	1.39	1.39	1.39	1.39	C3-C4-C5		120.54	120.28	119.74
C5-H8		1.08	1.07	1.09	C3-C4-O9			116.97	117.51
C6-H7		1.07	1.07	1.08	C5-C4-O9			122.75	122.75
O9-H10			0.95	0.96	C4-C5-C6		120.05	119.79	120.01
N13-C14		1.27	1.27	1.28	C4-C5-H8		120.34	120.38	120.07
C14-H15	1.08	1.08	1.08	1.10	C6-C5-H8		119.31	119.82	119.92
C14-C16	1.46	1.46	1.47	1.46	C1-C6-C5		120.65	120.59	121.04
C16-C17	1.39	1.39	1.39	1.41	C1-C6-H7	120.2	119.17	120.26	118.51
C16-C21	1.35	1.40	1.40	1.40	C5-C6-H7		119.18	119.12	120.44
C17-C18	1.42	1.39	1.39	1.38	C4-O9-H10			114.82	109.67
C17-H25	1.08	1.08	1.07	1.08	C1-N13-C14	118.1	119.5	123.38	120.59
C18-C19	1.34	1.39	1.39	1.41	N13-C14-H15		120.9	121.59	121.59
C18-H24	1.08	1.08	1.07	1.08	N13-C14-C16	123.6	123.34	122.86	123.09
C19-C20	1.34	1.40	1.39	1.40	H15-C14-C16		115.66	115.54	115.31
C19-O26		1.36	1.37	1.36	C14-C16-C17	119.1	119.62	119.91	121.97
C20-C21	1.41	1.38	1.38	1.39	C14-C16-C21	121.4	121.94	121.55	119.76
C20-H23	1.08	1.08	1.07	1.08	C17-C16-C21	121.6	118.43	118.54	118.27
C21-H22		1.07	1.07	1.09	C16-C17-C18	117.5	121.51	121.38	120.79
O26-C27		1.42	1.43	1.42	C16-C17-H25		119.48	119.74	118.60
C27-H28		1.09	1.08	1.10	C18-C17-H25		118.99	118.88	120.61
C27-H29		1.08	1.08	1.09	C17-C18-C19		119.51	119.17	120.30
C27-H30		1.09	1.08	1.10	C17-C18-H24		121.23	119.60	121.34
					C19-C18-H24		121.23	121.23	118.36
					C18-C19-C20	121.4	119.84	120.23	119.77
					C18-C19-O26		118.84	124.01	115.65
					C20-C19-O26			115.75	124.58
					C19-C20-C21	121.2	120.22	120.00	119.29
					C19-C20-H23		118.45	118.36	121.18
					C21-C20-H23		121.32	121.63	119.53
					C16-C21-C20		120.73	120.68	121.59
					C16-C21-H22		118.73	118.70	119.43
					C20-C21-H22		120.53	120.63	118.98
					C19-O26-C27		118.84	121.83	118.78
					O26-C27-H28		111.22	105.52	111.33
					O26-C27-H29		105.67	111.03	105.80
					O26-C27-H30		111.22	111.03	111.32
					H28-C27-H29		109.48	109.69	109.37
					H28-C27-H30		109.65	109.69	109.56
					H29-C27-H30		109.48	109.79	109.38

A: Calculated by B3LYP/6-31+G(d,p); B: Calculated by B3LYP/6-311++G(d,p) *Ref. 50, 51 #Ref. 1

$$\beta_{tot} = \left[\left(\beta_{xxx} + \beta_{xyy} + \beta_{xzz} \right)^2 + \left(\beta_{yyy} + \beta_{yzz} + \beta_{yxx} \right)^2 + \left(\beta_{zzz} + \beta_{zxx} + \beta_{zyy} \right)^2 \right]^{1/2}$$

The total static dipole moment, the mean polarizability, the anisotropy of the polarizability and the mean first-order hyperpolarizability of the title compound has been calculated using B3LYP/6-311++G(d, p) level. The conversion factor α, β in atomic and cgs units: 1 atomic unit (a.u.) =0.1482 x 10^{-24} electrostatic unit (esu) for α; 1 a.u. = 8.6393×10^{-33} esu for β.

The calculated dipole moment and hyperpolarizability values obtained from B3LYP with the basis set 6-311++G(d, p) method is collected in Table 5. Urea is

one of the prototypical molecules used in the study of the NLO properties of the molecular systems. Therefore it is used frequently as a threshold value for comparative purposes. The first order hyperpolarizability of pHNpMBA with B3LYP/6-311++G(d, p) basis set is 2.06×10^{-30} esu which is five and half times greater than the value of urea (β_{tot} = 0.372×10^{-30} esu). From the computation, the high values of the hyperpolarizability of pHNpMBA are probably attributed to the nonlinear optical (NLO) property of the molecule.

4.3 HOMO-LUMO analysis

The analysis of frontier molecular orbitals describes one electron excitation from the highest occupied molecular orbital (HOMO) to the lowest unoccupied molecular orbital (LUMO). The energy of HOMO is directly related to the ionization potential and the energy of LUMO is related to the electron affinity. The HOMO–LUMO energy gap is an important stability index and also it reflects the chemical activity of a molecule[64]. The MOs are defined as eigen functions of the Fock operator, which exhibits the full symmetry of the nuclear point group, and they necessarily form a basis for irreducible representations of full point-group symmetry. In the present study, the energies of HOMO, HOMO-1, HOMO-2, LUMO, LUMO+1 and LUMO+2 and their orbital energy gaps are calculated by B3LYP/6-311++G(d,p) method. The pictorial illustration of the frontier molecular orbitals and their respective positive and negative regions are shown in Fig. 3. In the HOMO

Table 5 – The calculated electric dipole moment μ(D), the average polarizability α(esu) and the first hyperpolarizability β_{tot} (esu)) of p-hydroxy-N-(p-methoxy benzylidene)aniline using B3LYP/6-311++G(d,p).

Parameters	B3LYP/6-311++G (d, p)	Parameters	B3LYP/6-311++G (d, p)	Parameters	B3LYP/6-311++G (d, p)
μ_x	0.667	α_{XX}	175.6718	β_{xxx}	-13.167
μ_y	-1.4841	α_{XY}	34.15309	β_{xxy}	-39.7373
μ_z	0.001	α_{YY}	342.4196	β_{xyy}	4.496797
μ(Debye)	1.6271	α_{XZ}	-3.00914	β_{yyy}	283.8209
		α_{YZ}	2.212319	β_{xxz}	3.124805
		α_{ZZ}	96.42178	β_{xyz}	0.923486
		α(esu)	3.0357E-23	β_{yyz}	4.315452
		Δα(esu)	$3.3416\text{x}10^{-23}$	β_{xzz}	35.69838
				β_{yzz}	-7.47203
				β_{zzz}	-5.20935
				β_{tot} (esu)	$2.0575\text{x }10^{-30}$

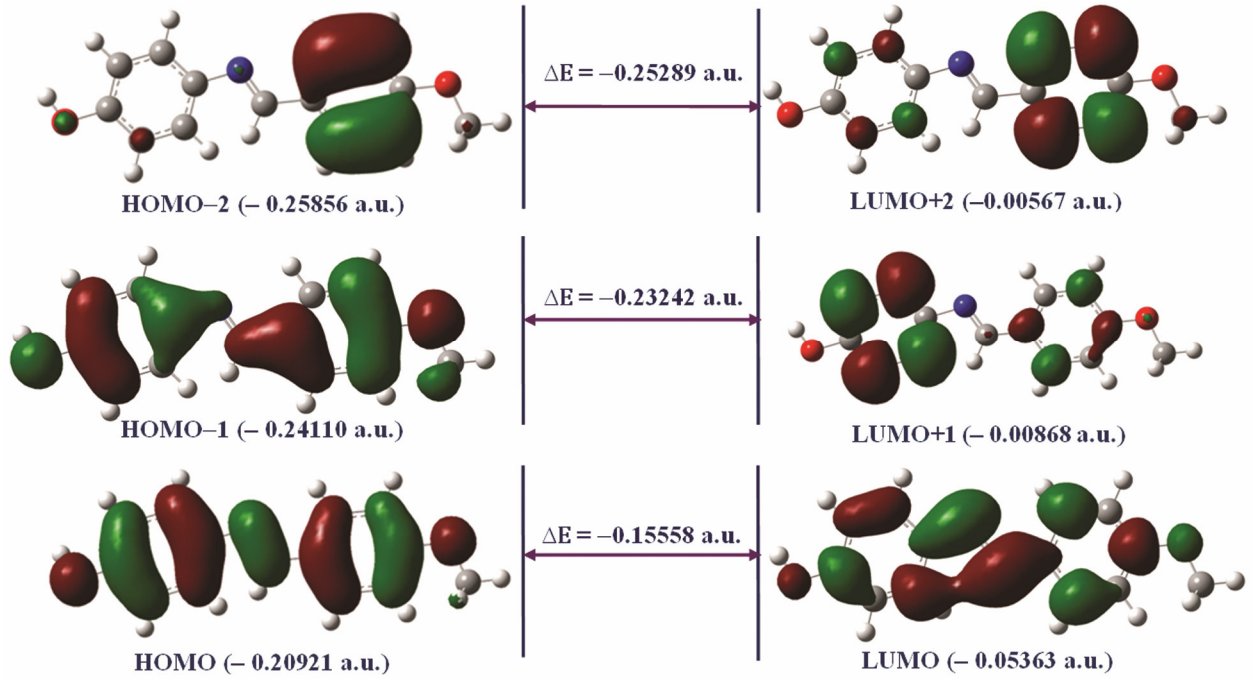

Fig. 3 – HOMO-LUMO plot of p-hydroxy-N-(p-methoxybenzylidene) aniline

surface, the bonding *p* orbitals spreading over the ring carbon atoms are helpful to hold the molecule together. It is worth mentioning here that the molecular orbital lobes which located on the chlorine atom of the HOMO surface is a non-bonding orbital. Hence, the electrons in chlorine atom act little like a lone pair of electrons in a Lewis structure. In contrast, the molecular orbital lobes on C3–H11 and C6–H7 bonds are σ orbitals and they have cylindrical symmetry about the inter-nuclear axis. The same type of σ orbital is also identified on the bond C2–H12 in LUMO + 1 surface. The molecular orbital lobes spreading over the HOMO - 2 and LUMO + 2 surfaces are of anti-bonding character because it has a node between adjacent nuclei with lobes of opposite sign (shown in different colors) and p-orbital on the carbon atom is a major contributor of HOMO - 2, LUMO + 2 surfaces. The energy gap between HOMO and LUMO explains the eventual charge transfer interaction within the molecule, which influences the biological activity of a molecule. In the case of pHNpMBA, the smallest energy gap of $\Delta E = -0.15558$ a.u. is identified between the HOMO and LUMO with the help of B3LYP/6-311++G(d,p) method.

4.4 Natural bond orbital analysis

The natural bond orbital (NBO) analysis[65] of pHNpMBA are being performed to estimate the delocalization pattern of electron density between the principle occupied Lewis-type (bond or lone pair) orbitals and uncoccupied non-Lewis (antibond or Rydberg) orbitals. Table 6 lists the occupancies and energies of most interacting NBO's along with their percentage of hybrid atomic orbital contribution. The interactions result is a loss of occupancy from the localized NBO of the idealized Lewis structure into an empty non-Lewis orbital. For each donor (i) and acceptor (j), the stabilization energy E(2) associated with the delocatziation $i \rightarrow j$ is estimated as:

$$E^{(2)} = -n\frac{\langle \sigma | F | \sigma \rangle^2}{\varepsilon_{\sigma^*} - \varepsilon_\sigma} = -n_\sigma \frac{F_{ij}^2}{\Delta E}$$

where $\langle \sigma | F | \sigma \rangle$ or F_{ij} is the Fock matrix element between the *i* and *j* NBO orbital, ε_σ and ε_{σ^*} are the energies of σ and σ* NBO's, and n_σ is the population of the donor σ orbital. NBO analysis provides an efficient method for studying intra and intermolecular bonding and interaction among bonds, and also provides a convenient basis for investigating charge-transfer or conjugative interaction in molecular systems. Some electron donor orbital, acceptor orbital and the interacting stabilization energy resulted from the second-order micro-disturbance theory are reported[66]. The larger the $E^{(2)}$ value, the more intensive is the interaction between electron donor and electron acceptors, i.e., the more donating tendency from electron donors to electron acceptors and the greater the extent of conjugation of the whole system. NBO analysis has been performed on the molecular pHNpMBA to

Table 6 – Second-order perturbation theory analysis of Fock matrix in NBO basic corresponding to the intra molecular bonds of p-hydroxy-N-(p-methoxybenzylidine)aniline

Donor (i)	ED (i) (e)	Acceptor (j)	ED (j) (e)	[a]$E^{(2)}$ (kJ mol^{-1})	[b]E(j) – E(i) (a.u.)	[c]F(i,j) (a.u.)
σ(C_1–N_{13})	1.97309	σ*(C_{14}–C_{16})	0.03824	5.31	1.10	0.068
σ(C_4–O_9)	1.99383	σ*(C_2–C_3)	0.01482	1.29	1.41	0.038
σ(C_9–H_{10})	1.98929	σ *(C_3–C_4)	0.02322	3.37	1.33	0.060
σ(N_{13}–C_{14})	1.98716	σ*(C_1–C_6)	0.02187	2.72	1.45	0.056
σ(C_{14}–H_{15})	1.98219	σ*(C_{16}–C_{17})	0.02305	2.67	1.13	0.037
σ(C_{14}–C_{16})	1.97317	σ*(C_1–N_{13})	0.02920	3.62	0.99	0.053
σ(C_{18}–C_{19})	1.97762	σ*(C_{19}–C_{20})	0.02634	4.01	1.29	0.064
σ(C_{19}–C_{20})	1.97810	σ*(C_{18}–C_{19})	0.02181	3.89	1.29	0.063
σ(C_{19}–O_{26})	1.98919	σ*(C_{20}–C_{21})	0.01522	1.41	1.40	0.040
σ(O_{26}–C_{27})	1.99329	σ*(O_{27}–H_{29})	0.00999	21.12	3.73	0.251
σ(C_{27}–H_{28})	1.99335	σ*(C_{27}–H_{30})	0.01770	26.48	5.48	0.341
σ(C_{27}–H_{29})	1.99129	σ*(C_{27}–H_{30})	0.01770	10.16	5.47	0.211
LP(1)O_9	1.98289	σ*(C_4–C_5)	0.02449	4.69	1.18	0.067
LP(1)N_{13}	1.92677	σ*(C_{14}–H_{15})	0.04282	9.00	0.84	0.078
LP(1)O_{26}	1.97189	σ*(C_{19}–C_{20})	0.02634	4.89	1.17	0.068
LP(2)O_9	1.89850	π*(C_3–O_4)	0.38876	18.87	0.38	0.081
LP(2)O_{26}	1.85676	π*(C_{19}–C_{20})	0.38795	23.60	0.33	0.084

$E^{(2)}$ means energy of hyperconjugative interactions.
[b] Energy difference between donor and acceptor *i* and *j* NBO orbitals.
[c] *F(i,j)* is the Fock matrix element between *i* and *j* NBO orbitals.

identify and explain the formation of the strong intramolecular hydrogen bonding between toluene group and carbon in the molecule. The corresponding results have been tabulated in Table 6. The importance of hyper-conjugative interaction and electron density transfer (EDT) from lone electron pairs of the Y atom to the (X–H) anti-bonding orbital in the X–H ...Y system have been reported by Reed *et al.*[67]. Table 6 shows calculated natural orbital occupancy (number of electron (or) "natural population" of the orbital). It is noted that the maximum occupancies 1.99383, 1.99335 and, 1.99329 and 1.9880 e are obtained for BD(C4–O9), BD(C27–H28) and BD(O26–C27), respectively. Therefore, the results suggest that the C4–O9, C1–N13 and C19–O26 bond lengths of these compounds are essentially controlled by the *p* character of these hybrids orbital's and also by the nature of the C4–O9, C1–N13 and C19–O26 bonds.

4.5 Molecular electrostatic potential (MEP) Surface

Molecular electrostatic potential (MEP) at a point in space around a molecule gives information about the net electrostatic effect produced at that point by total charge distribution (electron + proton) of the molecule and correlates with dipole moments, electro-negativity, partial charges and chemical reactivity of the molecules. It provides a visual method to understand the relative polarity of the molecule. An electron density is surface mapped with electrostatic potential surface depicts the size, shape, charge density and site of chemical reactivity of the molecules.

The different values of the electrostatic potential at the surface are represented by different colors; red represents regions of most electro negative electrostatic potential, blue represents regions of the most positive electrostatic potential and green represents region of zero potential. Potential increases in the order red < orange < yellow <green < blue. Such mapped electrostatic potential surface have been plotted for title molecule in B3LYP/6-311++G (d, p) basis set using the computer software Gauss view. Projections of these surfaces along the molecular plane and a perpendicular plane are given in Fig. 4. This figure provides a visual representation of the chemically active sites and comparative reactivity of atoms[68].

4.6 Vibrational spectral analysis

The vibrational analysis obtained for pHNpMBA with unscaled B3LYP/6-31+G(d,p) and B3LYP/6-311++G(d,p) force field are generally somewhat greater than the experimental values due to neglect of anharmonicity in real system. These discrepancies can be corrected either by computing anharmonic corrections explicitly or by introducing a scaled field or directly scaling the calculated wavenumbers with proper scale factor. A tentative assignment is often made on the basis of the unscaled frequencies by assuming the observed frequencies so that they are in the same order as the calculated ones. Then for an easier comparison to the observed values, the calculated frequencies are scaled by the scale to less than 1, to minimize the overall deviation. For better agreement we have utilized different scaling factors (0.9345 and 0.9786) for all fundamental modes to obtain the scaled frequencies of the compound. The resultant scaled frequencies are also listed in Table 7. Figures 5 and 6, present the experimental and theoretical FT-IR and FT-Raman spectra of pHNpMBA, respectively.

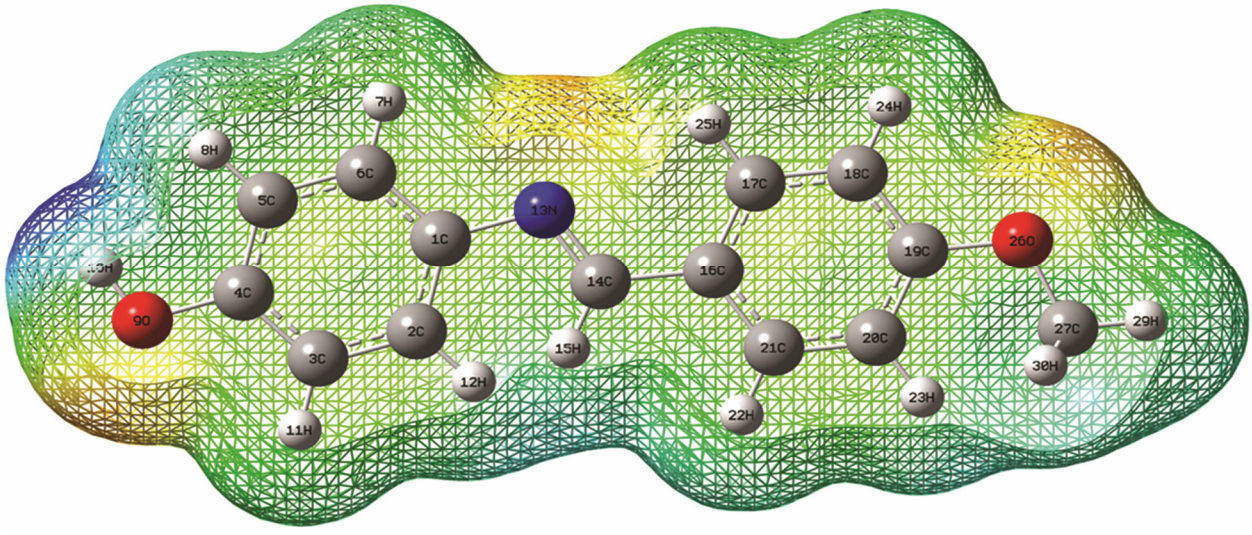

Fig. 4 – Electrostatic potential surface of p-hydroxy-N-(p-methoxybenzylidene)aniline

Table 7 – The observed FTIR, FT-Raman and calculated (unscaled and scaled) frequencies (cm^{-1}) and probable assignments of p-hydroxy-N-(p-methoxybenzylidine)aniline using B3LYP/6-31+G(d,p) and B3LYP /6-311++G(d,p)

Mode No.	Frequencies (cm^{-1})						Assignments/(% PED)
	Observed		Unscaled		Scaled		
(i)	FT-IR	FT-Raman	A	B	A	B	
1	3409		4048	3837	3412	3408	νOH(95)
2	3068		3414	3206	3074	3068	νCH(99)
3	3045		3411	3202	3049	3044	νCH(98)
4	3000		3402	3192	3007	3002	νCH(97)
5	2977		3396	3190	2981	2977	νCH(99)
6	2955		3392	3186	2959	2954	νCH(96)
7	2932		3380	3174	2933	2932	νCH(96)
8	2909		3351	3160	2913	2910	νCH(96)
9	2886		3349	3150	2890	2885	νCH(98)
10	2841		3343	3137	2845	2840	νCH(96)
11	2750		3277	3068	2756	2751	$\nu_{ass}CH_3$ (96)
12	2704		3230	3008	2705	2704	$\nu_{ass}CH_3$(98)
13	2659		3204	2997	2663	2660	$\nu_{ss}CH_3$(98)
14		1625	1884	1682	1628	1625	νCN(77), δCH(15)
15		1602	1822	1650	1607	1603	νCC(69), δCH(12)
16	1581		1815	1638	1586	1580	νCC(68), δCH(14)
17	1569		1788	1618	1572	1570	νCC(59), δOH(25), δCO(12)
18	1558	1557	1770	1603	1555	1558	νCC(58), δCO(20), νCN(10)
19	1512	1511	1702	1543	1516	1512	δCH(63), νCO(23), δCN(11)
20	1500		1694	1531	1507	1502	δCH(62), νCO(20), δCO(12)
21	1440	1443	1668	1505	1443	1440	$\delta_{ipb}CH_3$(88)
22	1429		1661	1494	1435	1428	$\delta_{opb}CH_3$(85)
23			1627	1475	1427	1422	$\delta_{sb}CH_3$(87)
24	1417		1604	1462	1422	1418	δCH(62), δOH(18), νCC(10)
25	1406	1409	1591	1452	1412	1410	δCH(60), δOH(21), νCC(12)
26		1341	1548	1405	1345	1340	δCH(54), νCO(21), δCN(10)
27	1336		1484	1357	1338	1335	δOH(71), δCH(20)
28	1324		1474	1346	1323	1324	νCC(54), δCO(21), δCC(12)
29	1289	1284	1423	1328	1290	1285	νCC(58), δCO(20)
30	1267		1392	1311	1269	1270	νCC(59), δCH(26)
31	1255		1385	1279	1260	1256	νCN(63), νCO(18), νCC(10)
32	1220	1216	1373	1277	1223	1219	νCO(78), δCH(16), δCO(10)
33			1357	1265	1216	1212	νCC(52), δCO(19), δCC(11)
34	1197	1193	1324	1216	1198	1194	νCO(60), νCN(15), νCC(10)
35	1185		1313	1202	1189	1185	$\delta_{opr}CH_3$(82)
36			1309	1189	1171	1165	δCH(58), δOH(17), νCC(10)
37			1304	1186	1163	1159	δCH(52), δOH(21), νCN(12)
38			1276	1179	1147	1140	δCH(56), δOH(22), νCO(10)
39	1127	1125	1253	1168	1128	1126	$\delta_{ipr}CH_3$(78), νCO(10)
40	1116		1236	1130	1120	1117	δCH(68), νCO(15), δCN(10)
41			1226	1121	1063	1060	δ_{ring} (66), νCO(18), δCN(10)
42	1035		1171	1057	1040	1036	νCC(59), νCN(12)
43			1155	1023	1023	1020	νCC(54), δCO(17), δCC(10)
44			1142	1023	994	990	νCO(68), δCH(26)
45	979	977	1139	1003	980	978	δCH(56), δOH(21)
46	968		1130	992	971	968	δCH(58), δOH(24), νCO(10)
47	933		1129	959	936	933	δCH(58), δOH(22)
48	887		1114	945	889	886	νCC(52), δCO(18)
49			1106	940	871	864	νCC(58), δCO(12)
50			993	895	859	853	δCN(49), νCC(25)

Contd—

Table 7 – The observed FTIR, FT-Raman and calculated (unscaled and scaled) frequencies (cm^{-1}) and probable assignments of p-hydroxy-N-(p-methoxybenzylidine)aniline using B3LYP/6-31+G(d,p) and B3LYP /6-311++G(d,p) — *Contd*

Mode No.	Frequencies (cm^{-1})						Assignments/(% PED)
	Observed		Unscaled		Scaled		
(i)	FT-IR	FT-Raman	A	B	A	B	
51	840		982	860	843	840	νCC(52), δCO(12)
52			964	855	827	823	δCN(52, νCC(25), δCO(10)
53			959	840	812	808	γCH(47), γCO(18)
54		784	945	817	788	783	γCH(49), γCC(17)
55	771		926	810	773	770	γCH(44), γCN(20)
56	747		873	807	744	746	γOH(47), γCO(12)
57	725		836	765	727	724	γCH(44), γCC(21)
58		704	819	742	708	704	γCH(47), γCO(20)
59	667		816	720	670	668	δCO(52), νCC(20), νCO(10)
60	632		728	658	634	630	δCO(52), νCC(18), νCO(10)
61		625	719	648	628	626	δCC(60), νCH(18)
62	597		654	605	599	598	γCH(70), γ_{ring}(18)
63	539		623	550	541	540	γCH(72), γ_{ring}(16)
64	515		596	532	517	516	δCO(55), $\delta_{ipr}CH_3$(78), δCH(10)
65		499	553	510	504	500	γCC(57), γ_{ring}(12)
66	493		540	496	497	493	γCH(59), γ_{ring}(10)
67	435		491	443	436	435	γCH(59), γ_{ring}(10)
68		420	484	433	424	421	δ_{ring}(68)
69			475	427	414	404	γCO(58)
70			456	414	375	370	γCN(61), γCH(15)
71		363	425	394	366	363	γCN(60)
72		317	393	349	321	318	δ_{ring}(48), δCN(13)
73			328	310	287	283	δ_{ring}(51), δCH(10)
74			310	300	263	260	$\gamma COCH_3$(55)
75		249	259	252	252	250	τCH_3(63)
76		203	233	221	209	201	γCO(55), γCH(15)
77			212	200	192	190	δ_{ring}(56), δCC(16)
78		180	206	192	188	182	δ_{ring}(45), δCH(18)
79		134	168	152	141	135	γ_{ring}(54), τCH_3(16)
80			121	118	98	95	γ_{ring}(48), γCO(14)
81			82	82	78	76	γ_{ring}(48), γCO(14)
82			54	50	50	48	γ_{ring}(44), γCH(16)
83			39	39	36	35	γ_{ring}(49), γOH(14)
84			35	32	28	27	γ_{ring}(47), γCO(10)

4.6.1 O–H vibrations

The OH group gives rise to three vibrations, stretching, in-plane bending and out-of-plane bending vibrations. The OH group vibrations are likely to be the most sensitive to the environment, so they show pronounced shifts in the spectra of the hydrogen bonded species. In the case unsubstituted phenol it has been shown that the frequency of OH stretching vibration in the gas phase is 3657 cm^{-1} (Ref. 69). In our case a very strong band in FT-IR spectrum 3409 cm^{-1} is assigned to OH stretching vibration. A comparison of these band with literature data predict that there is negative deviation may be due to the fact that the presence of strong intramolecular hydrogen bonding. However, the calculated value by B3LYP/6-311++G(d,p) level shows at 3408cm^{-1}. The OH in-plane bending vibration in phenol, in general lies in the region 1225 – 1250 cm^{-1} and is not much affected due to hydrogen bonding unlike the stretching and out-of plane deformation frequencies[70]. The medium strong infrared frequency at 1220 cm^{-1} and Raman frequency at 1216 cm^{-1} is attributed is vibration. The theoretically computed value at 1219 cm^{-1} is exactly coincides with the experimental observations. The OH out-of-plane deformation vibration in phenol lies in the region 290-320 cm^{-1} for free OH and in the region 517-710 cm^{-1} for associated OH[70]. In both intermolecular and intramolecular association, the frequency is at a higher value that in free OH. The frequency increase with hydrogen bond strength

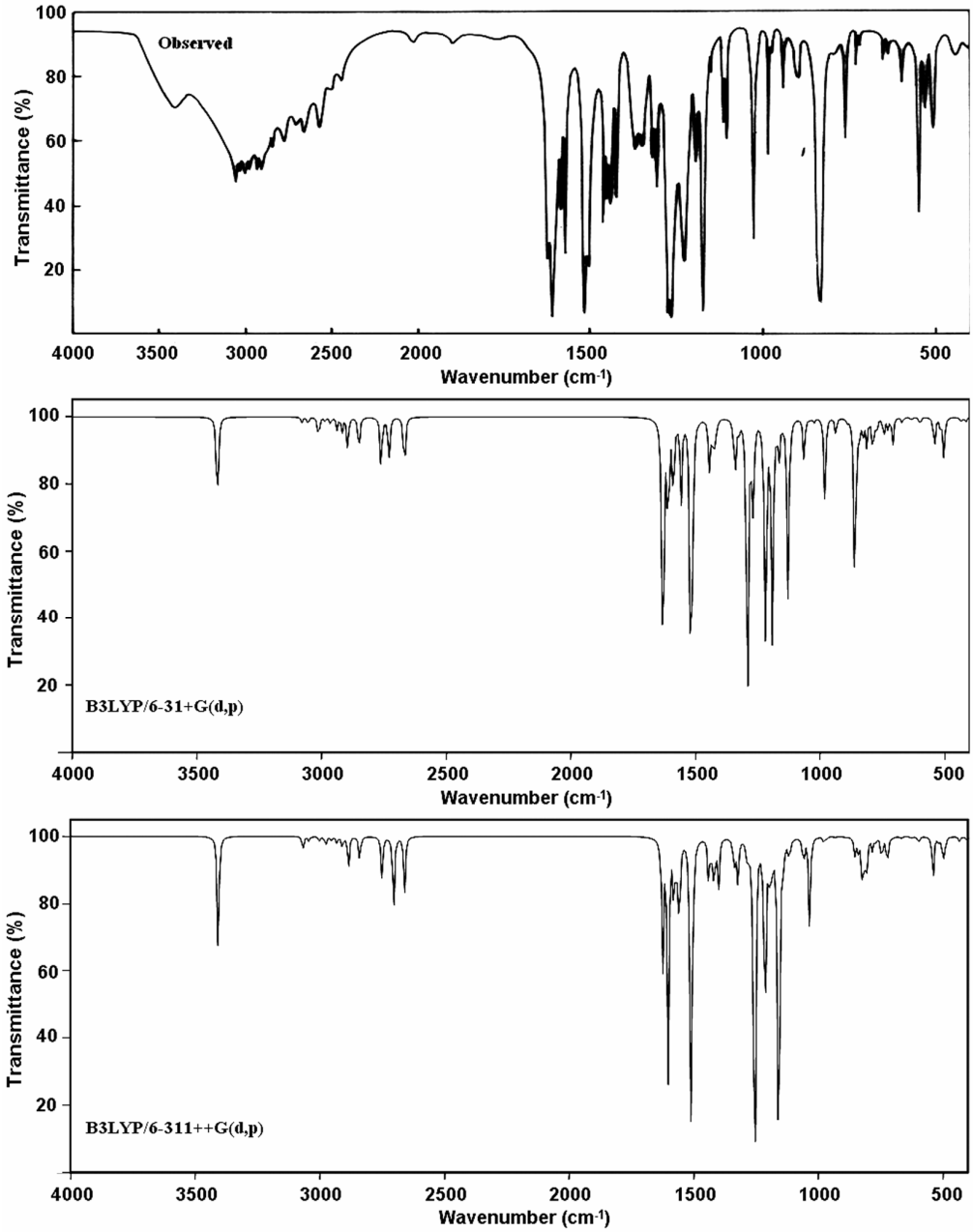

Fig. 5 – Observed and calculated infrared spectrum of p-hydroxy-N-(p-methoxybenzylidene)aniline

because of the larger amount of energy required to twist the OH bond out-of-plane [70]. In our case the Raman band at 317 cm^{-1} is assigned as OH out-of-plane bending vibration. The calculated value of this vibration at 318 cm^{-1} is good agreement with experimental value.

4.6.2 C–H vibrations

For simplicity, modes of vibrations of aromatic compounds are considered as separate C–H or ring C–C vibrations. However, as with any complex molecules, vibrational interactions occur and these levels only indicate the predominant vibration. Substituted benzenes have large number of sensitive bands, i.e., bands whose position is significantly affected by the mass and electronic properties, mesomeric or inductive of the substituents. According to the literature[71,72], in infrared spectra, most mononuclear and polynuclear aromatic compounds have three or four peaks in the region 3000–3100 cm^{-1}, these are due to the stretching vibrations of the ring CH bands. Accordingly, in the present study, the FT-IR bands identified at 3068, 3045, 3000, 2977,

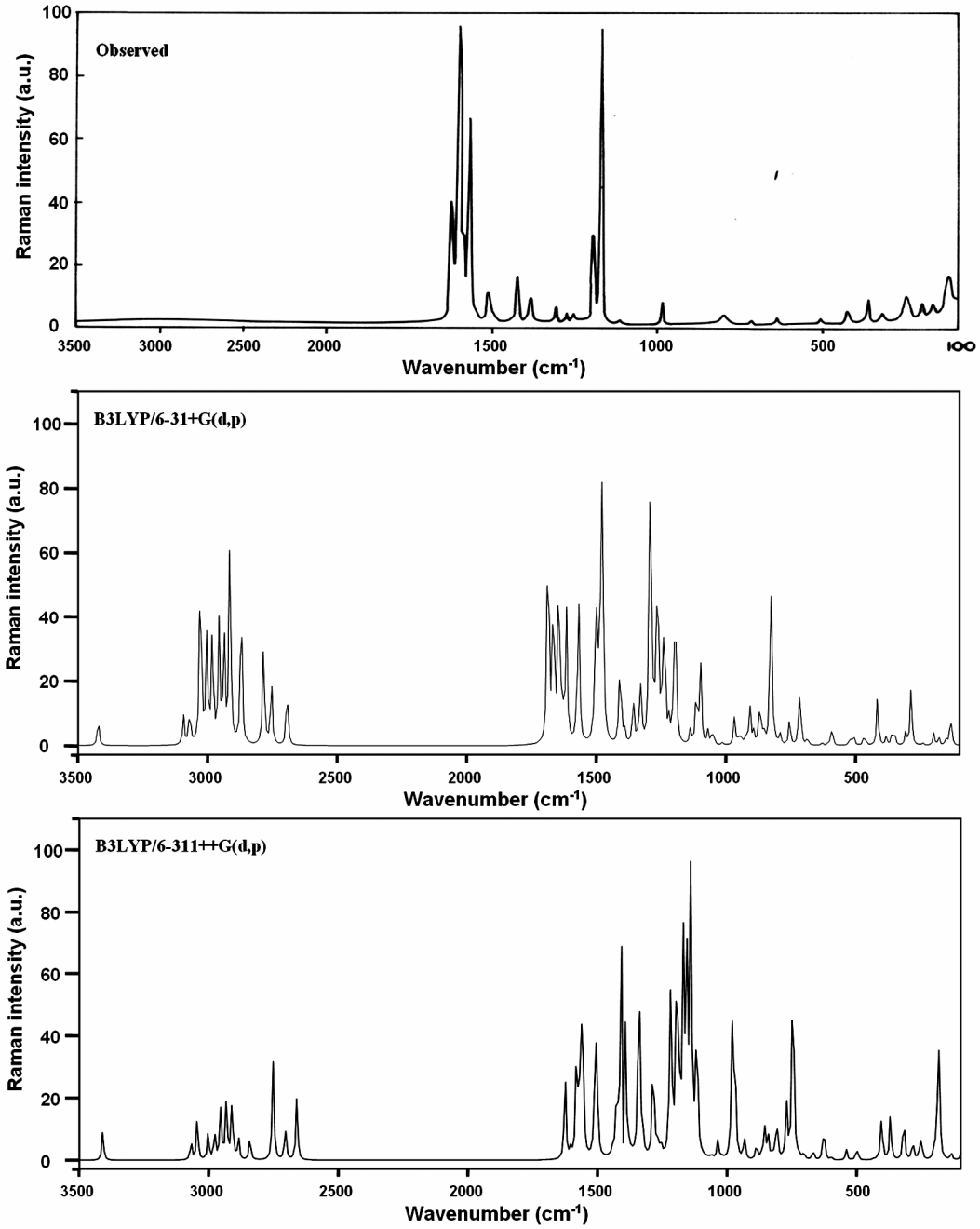

Fig. 6 – Observed and calculated Raman spectrum of p-hydroxy-N-(p-methoxybenzylidene)aniline

2950, 2932, 2909, 2886 and 2659cm^{-1} are assigned to C–H stretching vibrations of pHNpMBA. In B3LYP/6-311++G (d, p) method the values calculated at 3068, 3044, 3002, 2977, 2954, 2932, 2910, 2885, 2660 cm^{-1}. The FT-IR bands at 1512, 1500, 1417, 1406, 1116, 979, 968 and 933 cm^{-1} and the FT Raman bands at1511, 1409, 1341, 977 cm^{-1} are assigned to C–H in-plane bending vibration of pHNpMBA. The C–H out-of-plane bending vibrations of the pHNpMBA are well indentified at 771, 725, 597, 539, 493, 435 cm^{-1} in the FT-IR and 784, 704 cm^{-1} in the FT-Raman spectra which are found to be well within their characteristic region.

4.6.3 Methyl group vibrations

The title compound under consideration possesses a CH_3 group in the side-substituted chain. For the assignments of CH_3 group frequencies, one can expect that nine fundamentals can be associated with each CH_3 group, namely the symmetrical stretching in CH_3

(CH_3 symmetric stretch) and asymmetrical stretching (CH_3 asymmetric stretch) in-plane stretching modes (i.e., in-plane hydrogen stretching mode); the symmetrical (CH_3 symmetric deform) and asymmetrical (CH_3 asymmetric deform) deformation modes; the in-plane rocking (CH_3 ipr), out-of-plane rocking (CH_3 opr), and twisting (tCH_3) modes. Methyl groups are generally referred as electron-donating substituent in the aromatic ring system. The methyl hydrogen atoms are subjected simultaneously to hyper conjugation and back donation, which causes the decrease in stretching wave numbers and infrared intensities, as reported in literature[73] for similar molecular system. For the O–CH_3 group compounds[74] the symmetric stretching mode appears in the range 2825–2870 cm^{-1}, lower in magnitude compared with the value in CH_3 compounds (2860–2935 cm^{-1}), whereas the asymmetric stretching modes lie in the same region, 2924 and 2985 cm^{-1}. In the present study, the asymmetric and symmetric stretching vibrations of CH_3 group have been identified at 2840, 2751 and 2704 cm^{-1} by B3LYP/6-311++G (d, p) method. The recorded FT-IR spectrum show two weak bands observed at 2841, 2750 and 2704 cm^{-1}, which are assigned to C–H asymmetric and symmetric vibrations of a CH_3 group for the title compound. The in-plane and out-of-plane rocking vibrations for CH_3 group have been calculated at 1126 and 1194 cm^{-1} by B3LYP/6-311++G(d, p) method. The asymmetrical CH_3 deformation vibrations are computed by B3LYP++G(d, p) method at 1440 cm^{-1}. Similarly, the symmetrical deformation vibration of CH_3 group is computed at 1428 cm^{-1} for pHNpMBA. The bands observed at 1440 and 1443 cm^{-1} FT-IR and FT-Raman spectra, respectively.

4.6.4 C–C vibrations

The ring C=C and C–C stretching vibrations, known as semicircle stretching usually occur in the region 1400–1625 cm^{-}. Hence in the present[1,75,76] investigation, the FT-IR bands indentified at 1581, 1569, 1558, 1324, 1289, 1267 cm^{-1} and the FT-Raman bands at 1602, 1557, 1284 cm^{-1} are assigned to C–C stretching vibrations. The band ascribed at 625 and 499 cm^{-1} in FT-Raman spectrum have been designated to CC in-plane and out-of-plane bending mode. The calculated bending modes found at 626 cm^{-1} and 500 cm^{-1} in B3LYP/6-311++G(d, p) are assigned to C–C in-plane and out-of-plane bending vibrations, respectively.

4.6.5 O–CH_3 vibrations

The O–CH_3 mode is assigned to ~ 1040 cm^{-1} for anisole[77] and to the region 1000–1100 cm^{-1} for anisole and its derivatives[78,79]. This mode is assigned to 1026, 909 and 995 cm^{-1} for *o-, m-* and *p*-methoxy benzaldehyde, respectively. In the present investigation, the O–CH_3 stretching mode is theoretically identified value at 990 cm^{-1} using B3LYP/6-311++G(d, p) basis set. The C–O–CH_3 bending mode is assigned near 300 cm^{-1} for anisole by Owen and Hester[80] and at 421 cm^{-1} for *p*-methoxy benzaldehyde by Compagnaro and Wood[81]. Ramana Rao and co-workers[82] have proposed assignment for this mode in the region 300–670 cm^{-1} for anisole and its derivatives. As this mode lies in the region of the ring planar C–C–C angle bending modes, a strong mixing among these two modes and other planar modes is expected. Krishnakumar *et al.*[72] Assigned C–O–CH_3 angle bending mode at 341, 382 and 430 cm^{-1} for the *o- , m-* and *p*-methoxy-benzaldehydes, respectively. In accordance with above we have assigned the theoretically computed values by B3LYP/6-311++G(d, p) method at 630 cm^{-1} for the title compound as C–O–CH_3 angle bending mode, the value that coincides with 632 cm^{-1} band observed in FT-IR spectrum. The torsion mode of the O–CH_3 group was observed for anisole at 100 cm^{-1} by some workers[83]. The computed value predicted by B3LYP/6-311++G(d, p) method at 260 cm^{-1} for O–CH_3 torsion mode for pHNpMBA.

4.6.6 C–N and C=N vibrations

The identification of C–N and C=N stretching vibrations are a difficult task since the mixing of several modes are possible in the region. Silverstein[83] assigned C–N and C=N stretching absorption in the region 1386–1266 cm^{-1} and 1690–1630 cm^{-1}, respectively. Hence, in the present investigation, the band at 1625 cm^{-1} in FT-Raman spectrum assigned to C=N stretching vibration. The theoretically computed value at 1628 cm^{-1} and 1625 cm^{-1} by B3LYP/6-31+ G(d, p) and B3LYP/6-311++ G(d, p) methods, respectively for C=N stretching vibration. The band at 1255 cm^{-1} in FT-IR spectrum assigned to C–N stretching vibrations. The computed value for C–N stretching mode found at 1260 cm^{-1} and 1256 cm^{-1}, respectively in B3LYP/6-31+ G(d, p) and B3LYP/6-311++ G(d, p) methods.

5 Conclusions

The vibrational characteristics of pHNpMBA has been investigated by the experimental (FT-IR and FT-Raman)

and theoretical DFT quantum chemical methods. Scaled theoretical wave numbers and PED results were quite useful for the reliable assignments of normal modes of vibrations; moreover, the optimized geometrical parameters were calculated. On the basis of agreement between the calculated and experimental results, assignments of all the fundamental vibrational modes of the title compound are examined and proposed in this investigation. Therefore, the assignments made at higher level of theory with higher basis set with only reasonable deviations from the experimental values, seems to be correct. Based on calculated energy differences, the C4 conformer is found to be the most stable conformer. The electric dipole moments and first hyper polarizability of the compound studied have been calculated by DFT method with 6-311++G(d, p) basis set. The DFT calculated non-zero μ value of this legend shows that the pHNpMBA compound might have microscopic first hyperpolarizability with non-zero values obtained by the numerical second derivatives of the electric dipole moment according to the applied field strength. The NBO analysis performed in this study enabled us to know about the conjugative interactions and other type of interactions taking place within the molecular species. The second-order perturbation theory results show that the CH_3 group behaves as separate unit with sufficient interaction energy. The mapped iso-density surfaces for the frontier molecular orbitals were also plotted and the smallest energy gap of -0.15558 a.u. is calculated between HOMO and LUMO orbitals. The lowering of HOMO–LUMO band gap supports bioactive property of the molecule.

Acknowledgments

The authors are thankful to SAIF, Indian Institute of Technology, Chennai for getting recorded FT-IR and FT-Raman spectra. One of the authors (B Revathi) is grateful to the UGC-MRP [MRP-5128/149 (SERO/UGC)] for the financial assistance.

References

1 Balachandran V, Santhi G, Karpagam V & Lakshmi A, *J Mol Struct*, 1047 (2013) 249.
2 Diaz F A, Sanchez C O, Del Valle M A, Torres J L & Tagle LH, *Synth Met*, 118 (2001) 25.
3 Ng S C & Xu L, *Adv Mater*, 10 (1998) 1525.
4 Misra R A, Dubey S, Prasad B M & Singh D, *Indian J Chem*, 38 (1999) 141.
5 Prevast V, Petit A & Pla F, *Synth Met*, 104 (1999) 79.
6 Kanungo M, Kumar A & Contractor A Q, *J Electroanal Chem*, 528 (2002) 46.
7 Inzelt G & Kertesz V, *Electro Chim Acta*, 42 (1997) 229.
8 Dong Y & Mu S, *Electro Chim Acta*, 36 (1991) 2015.
9 Delongchamp D M & Hammond P T, *Chem Mater*, 16 (2004) 4799.
10 Whysner J, Vera L & Williams G M, *Pharmacol Ther*, 71 (1996) 107.
11 Hohenberg P & Kohn W, *Phys Rev B*, 136 (1964) 864.
12 Vaschetto M E, Retamal B A & Monkman A P, *J Mol Struct*, 468 (1999) 209.
13 Tzeng W B, Narayanan K, Lin J L & Tung C C, *Spectro Chim Acta*, 55 (1999) 153.
14 Tzeng W B, Narayanan K, Shieh K C & Tung C C, *J Mol Struct*, 428 (1998) 231.
15 Hohenberg P & Kohn W, *Phys Rev B*, 136 (1964) 864.
16 Evans J C, *Spectro Chim Acta*, 16 (1960) 428.
17 Roussy G & Nonat A, *J Mol Spectrosc*, 118 (1985) 180.
18 Lister G D, Tyler J K, Hog J H & Larsen N W, *J Mol Struct*, 23 (1974) 253.
19 Fukuyo M, Hirotsu K & Higuchi T, *Acta Crystallogr*, 38 (1982) 640.
20 Ventura M C & Kassab E, *Spectro Chim Acta*, 50 (1994) 69.
21 Gorse A D & Pesquer M, *J Mol Struct*, 21 (1993) 281.
22 Bock C W, George P & Trachtman M, *Theor Chim Acta*, 69 (1986) 235.
23 Wang Y, Saeb S & Pittman C U, *J Mol Struct*, 91 (1993) 281.
24 Altun A, Gokuk K & Kumru M, *J Mol Struct*, 625 (2003) 17.
25 Yudakul S & Sen A I, *Vib Spectrosc* 20 (1999) 27.
26 Alkalin E & Akyuz S, *J Mol Struct*, 175 (1999) 428.
27 Lopez Tocon I, Becucci M, Pietra Perzia G, Castelluchi E & Otero J C, *J Mol Struct*, 421 (2001) 565.
28 Vaschettom M E, Retamal B A & Monkman A P, *J Mol Struct*, 468 (1999) 209.
29 Palafox M A, Nunez J L & Gil M, *J Mol Struct*, 593 (2002) 101.
30 Tzeng W B & Narayanan K, *J Mol Struct*, 434 (1998) 247.
31 Engelter C, Thornton D A & Ziman M R, *J Mol Struct*, 49 (1978) 7.
32 Engelter C, Thornton D A & Ziman M R, *J Mol Struct* 119 (1976) 33
33 Johnson P R & Thornton D A, *Chimia*, 28 (7) (1974) 345.
34 Altun A, Golcuk K & Kumru M, *J Mol Struct*, 673 (2003) 155.
35 Sharma S J & Dwivedi C P D, *Indian J Pure Appl* Phys, 13 (1975) 570.
36 Sundaraganesan N, Saleem H, Mohan S & Ramalingam M, *Spectrochim Acta A*, 61 (2005) 377.
37 Shankar R, Yadav R A, Singh I S & Singh O N, *Indian J Pure Appl Phys*, 23 (1985) 339.
38 Barluenga J, Fananas F J, Sanz R & Fernandez Y, *Chem Eur J*, 8 (2002) 2034.
39 Rai A K, Kumar S & Rai A, *Vib Spectrosc*, 42(2006) 397.
40 Rai V K, Rai A, Rai D K & Rai S B, *Spectrochim Acta*, 60 (2004) 53.
41 Frisch M J, Trucks G W & Schlegel H B, *Gaussian*, (Inc, Wallingford CT), 2009.
42 Pulay P, Fogarasi G, Pongor G, Boggs J E & Vargha A, *J Am Chem Soc*, 105 (1983) 7037.
43 Rauhut G & Pulay P, *J Phys Chem*, 99 (1995) 3093.
44 Sundius T, *J Mol Spectrosc*, 82 (1980) 138.
45 Sundius T, *J Mol Struc*, 218 (1990) 321.

46 Sundius T, MOLVIB: *A program for Harmonic Force Fields Calculations*, QCPE Program No 604, 1991.
47 Polavarapu P L, *J Phys Chem*, 94 (1990) 8106.
48 Keresztury G, Holly S, Varga J, Besenyei G, Wang A V & Durig J R, *Spectrochim* Acta, 49 (1993) 2007.
49 Keresztury G, Chalmers J M & Griffiths P R, *Handbook of vibrational spectroscopy*, Vol 1, (John Wiley & Sons, Ltd), 2002.
50 Roussy G & Nonat A, *J Mol Spectrosc* 118 (1986) 180
51 Schultz G, Portalone G, Ramondo F, Domenicano A & Hargittai I, *Struct Chem*, 7 (1996) 59.
52 Prasad J V, Rai S B & Thakur S N, *Chem Phys Lett*, 164 (1989) 629.
53 Ahmed M K & Henry B R, *J Phys Chem*, 90 (1986) 629.
54 Tzeng W B, Narayan K, Lin J L & Tung C C, *Spectrochim Acta*, *A*,55 (1999) 153.
55 Sun X, Hao Q L, Wei W X, Yu Z X, Lu D D, Wang X & Wang Y S, *J Mol Struct Theochem*, 74 (2009) 904.
56 Andraud C, Brotin, Garcia T, Pelle F, Goldner P, Bigot B & Collet A, *J Am Chem Soc*, 116 (1994) 2094.
57 Geskin V M, Lambert C & Bredas J L, *J Am Chem Soc*, 125 (2003) 15651.
58 Nalano M, Fujita H, Takahata M & Yamaguchi K, *J Am Chem Soc*, 124 (2002) 9648.
59 Sajan D, Joe I H, Jayakumar V S & Zaleski J, *J Mol Struct*, 785 (2006) 43.
60 Zhang C R, Chen H S & Wang G H, *Chem Res Chin Univ*, 20 (2004) 640.
61 Sun Y, Chen X, Sun L, Guo X & Lu W, *J Chem Phys Lett*, 381 (2003) 397.
62 Christiansen O, Gauss J & Stanton J F, *J Chem Phys Lett*, 305 (1999)147.
63 Kleinman D A, *Phys Rev*, 126 (1962) 1977.
64 Srivastava A, Tandon P, Jain S & Asthana B P, *Spectrochim Acta A*, 84 (2011) 144.
65 Glendening E D, Landis C R & Weinhold F, *WIREs Comput Mol Sci*, 2 (2012) 1.
66 Liv J N, Chem Z R & Yuan S F, *J Zhejiang Unit Sci B*, 6 (2005) 584.
67 Reed A E, Curtiss L A & Weinhold F, *Chem Rev*, 88 (1988) 896.
68 Gupta V P, Sharma A, Virdi V & Ram VJ, *Spectrochim Acta A*, 64 (2006) 57.
69 Michalska D, Dienko D C, Abkowicz-Bienko A J & Latajka Z, *J Phys Chem*, 100 (1996) 123.
70 Varasanyi G, *Assignments of Vibrational spectra of seven hundred benzene derivatives,* (Wiley, New York), 1974.
71 Socrates G, *Infrared and raman characteristic group frequencies*: 3rd Ed (Wiley, New York), 2001.
72 Krishna Kuamr V & Balachandran V, *Spectrochim Acta*, 63A (2006) 464.
73 Smith B, *Infrared spectral interpretation*, *a systematic approach*, (CRC, Washington DC), 1999.
74 Singh D N, Singh I D & Yadav R A, *Ind J Phys*, 763 (2002) 307.
75 Krishnakumar V & John Xavier R, *Indian J Pure Appl Phys*, 41 (2003) 95.
76 Furic K, Mohacek V, Bonifacic M & Stefanic I, *J Mol Struct*, 267 (1992) 39.
77 Walter J & Balfour, *Spectrochim Acta*, 39 (1983) 795.
78 Owen N L & Hester R E, *Spectrochim Acta*, 25 (1969) 343.
79 Campangnaro G E & Wood J L, *J Mol Struct*, 6 (1970) 117.
80 Owen N L & Hester R E, *Spectrochim Acta*, 25 (1969) 343.
81 Campangnaro G E & Wood J L, *J Mol Struct*, 6 (1970) 117.
82 Venkkatram Reddy B, Ramana Rao G, *Vib Spectro*, 6 (1994) 231.
83 Silverstein M, Clayton Basseler G & Morill C, *Spectrometric identification of organic compounds,* (Wiley, New York), 1981.